Pressure and Stress Transients in Autoinjector Devices

Jean-Christophe Veilleux · Joseph E. Shepherd

This is a pre-print of an article published in the Journal of Drug Delivery and Translational Research. The final authenticated version is available online at: https://doi.org/10.1007/s13346-018-0568-7.

Abstract Spring-actuated autoinjectors delivering viscous drug solutions resulting from large drug concentrations require large spring forces which can create high peak pressures and stresses within syringes. The high peak pressures and stresses can lead to device failure. Measurements with a suite of novel instrumentation and analysis using numerical simulation explain the peak pressures and peak stresses as originating from mechanical impacts between moving components, the large acceleration of the components, and surprisingly, the production of tension waves in the liquid resulting in cavitation. The presence and intensity of cavitation depends on relative timing between the pressurization and the acceleration of the syringe, which, in turn, depends on the size and location of an air gap inside the syringe. We show that production of localized but very high pressures can result from shock wave focusing in the conical section of the syringe.

Keywords Autoinjector · Viscous drug solution · High concentration drug solution · Pressure waves · Stress waves · Cavitation · Shock focusing

1 Introduction

Autoinjectors were first developed and introduced for military applications in the 1970s for the delivery of emergency drugs in the field [16]. Today, autoinjectors are also used by civilians for emergency purposes (e.g., epinephrine), but they are also extensively used for long-term treatments requiring the frequent subcutanenous injection of biopharmaceuticals (e.g., etanercept, adalimumab and darbepoetin alfa) [2].

The volume of a subcutaneous injection is limited to approximately 1.0-1.5 mL [1, 9, 20] because subcutaneous tissues can only absorb a finite quantity of liquid. Exceeding an injection volume of 1.5 mL generally creates some discomfort due to the accumulation of liquid under the skin [9]. Typical autoinjectors use a 1 mL syringe [9, 21], and the maximum injection time a patient is willing to tolerate is typically around 10 to 15 seconds [9, 10].

The force required to extrude a volume V of drug solution within a time T can be estimated assuming a steady Poiseuille flow through the needle [15]. The required force F or syringeability is:

$$F = 32\,\mu\,l\left(\frac{D^2}{d^4}\right)\left(\frac{V}{T}\right)\ , \tag{1}$$

where μ is the viscosity of the drug solution, D is the inner diameter of the syringe's barrel, and d and l are respectively the inner diameter and the length of the needle.

Equation 1 shows that for a given combination of syringe, needle, injection time and volume, the required force increases linearly with viscosity. This has significant implications for device design for high concentration drug formulations with high viscosities. The constraints on injection time and needle size mean that increasing the force F is the only practical alternative to inject newly developed drug solutions with viscosities as large as 25-30 cP [9].

Even if the specific design of each autoinjector device may differ, in most devices currently available on the market, the mechanism is spring actuated [9, 22, 23]. Activation of the device may result in mechanical impacts between the moving components of the autoinjector mechanism, and large accelerations/decelerations of the moving components may occur. This can be an issue when very viscous drug solutions are to be injected: the large syringeability of the drug (see Eq. 1) means that stiff springs must be used to power the autoinjector. When this is the case, the spring forces can result in impact velocities and accelerations/decelerations which are large enough to cause failure of the device [10, 21]. Peak pressures in excess of 6.9 MPa are believed to exist within autoinjectors upon actuation [19].

Although the potential issues associated with the use of very viscous drugs in autoinjectors have been acknowledged in the literature, no detailed study of the pressure and stress transients produced upon actuation

Communicating author: J.-C. Veilleux
Graduate Aerospace Laboratories
California Institute of Technology
1200 E. California Blvd., Pasadena, CA USA 91125
E-mail: jc.veilleux@caltech.edu

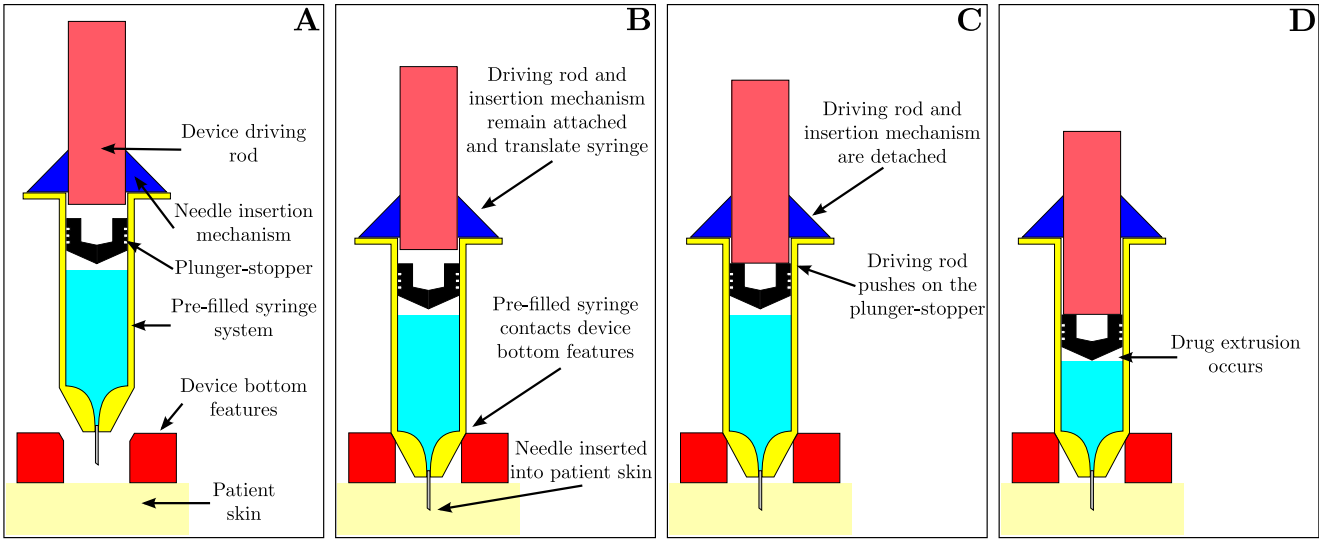

Fig. 1 Schematic of the actuation sequence of a typical autoinjector device.

has been performed. There is a lack of detailed understanding of how the key design parameters affect the device performances [25], and further research and development is needed to extend the range of operation of autoinjectors with respect to viscosity [1]. There is also a need for physical measurements on actual devices [23].

This has led us to investigate the pressure and stress transients in an autoinjector experimentally. We have developed novel techniques where miniature pressure transducers and miniature strain gauges are used to measure the liquid pressure and the strains in the glass syringe during actuation of an autoinjector. High speed digital video cameras are also used to visualize and analyze the motion of the various components within the autoinjector. The goal of this research is to develop a better understanding of the failure modes of the autoinjectors in order to improve upon the current designs, and to make autoinjectors more robust and reliable. Ultimately, this deeper understanding of the mechanics of autoinjectors will make it possible to use those devices to safely inject the increasingly viscous drug solutions under development.

The origin of the pressure and stress transients which can occur in an autoinjector will first be discussed qualitatively in this paper. Then, the experimental methods used to measure those transients will be described. This will be followed with some results and discussions. To end, the findings will be summarized in the conclusion.

2 Generation of Pressure and Stress Transients

Most autoinjectors are responsible for two main functions: 1) insertion of the needle into the patient; 2) delivery of the medicament to the patient. For the purpose of the present discussion, the sequence of events depicted in Fig. 1 will be considered. The concepts and explanations presented herein can however be adapted to autoinjectors which operate differently.

Figure 1 is a simplified schematic of the internal components and actuation sequence of an autoinjector. In panel A the device is in its initial state just before actuation. The needle shield has been removed, and the device bottom features are in contact with the patient's skin. The pre-filled syringe is mounted inside the device and it is sealed by a plunger-stopper. In panel B the device has been activated, and the spring-actuated driving rod is moving forward. The insertion mechanism attached to the driving rod is in contact with the syringe and accelerates the syringe forward. This inserts the needle into the patient. Once the needle reaches the adequate depth for injection the syringe is decelerated to a complete stop. In panel C the driving rod is moving independently from the insertion mechanism, and it impacts on the plunger-stopper. The force exerted by the spring-actuated driving rod on the plunger-stopper pressurizes the syringe and the medicament is extruded through the needle as shown in panel D.

In the sequence of events described above there are three events which are capable of producing significant pressure and stress transients in the syringe: 1) the syringe acceleration; 2) the syringe deceleration; 3) the impact of the spring-actuated driving rod on the plunger-stopper. The origin of the pressure and stress transients which can be generated by each of the three events will be introduced in this section. More details on these events will be provided in section 4 along with experimental results.

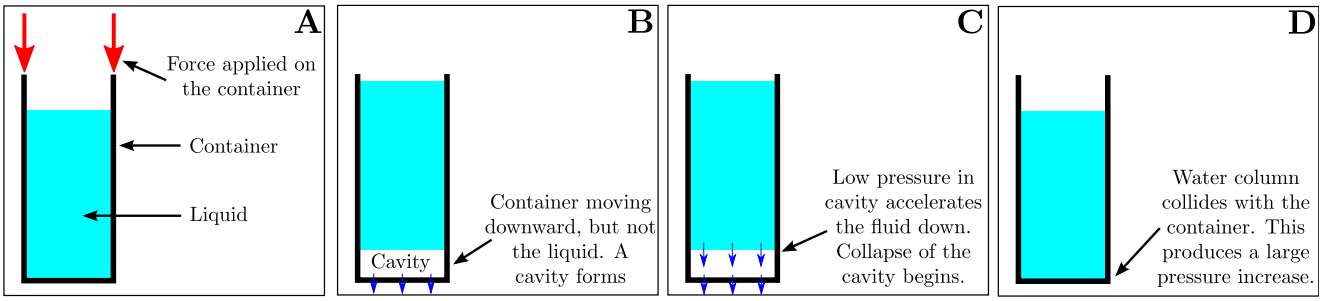

Fig. 2 Schematic of the growth and collapse of a cavity following the abrupt acceleration of a liquid-filled syringe.

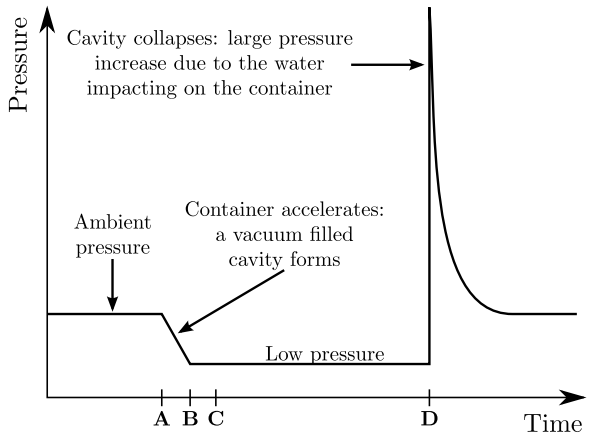

Fig. 3 Pressure at the bottom wall of a liquid-filled syringe which is impulsively accelerated. The events labeled from A through D correspond to the events shown in Fig. 2.

2.1 Syringe Acceleration (Event 1)

Upon device actuation the needle insertion mechanism impulsively accelerates the syringe forward. The acceleration of the syringe can be substantial (i.e., 10^3 to 10^4 m/s^2). Although the syringe is impulsively accelerated as soon as the insertion mechanism is released, the liquid contained inside the syringe is not. The acceleration of the liquid is lagging behind the acceleration of the syringe, and cavitation occurs at the bottom of the syringe [4, 8]; a cavity forms at the bottom of the syringe. This is schematically depicted using Fig. 2 where a liquid-filled container with a flat bottom wall is used for illustration. The pressure inside the cavity forming at the bottom wall is sub-atmospheric. This results in the production of tension waves in the liquid which progressively accelerate the liquid forward until the cavity collapses with great intensity. The collapse of the cavity produces a large and abrupt pressure increase as the liquid impacts on the bottom wall of the container.

A qualitative example of the liquid pressure history at the bottom of the container is shown in Fig. 3. The large and momentarily increase in liquid pressure creates stresses and strains in the walls of the syringe.[1]

2.2 Syringe Deceleration (Event 2)

The deceleration of the syringe upon reaching the right penetration depth for the needle (see Fig. 1B) can be substantial, as high as 10^3 to 10^4 m/s^2. The fluid and the solid elements near the point of contact come to a stop abruptly, but the fluid and the solid elements away from the point of contact are not immediately decelerated. Instead, they are decelerated upon arrival of compression waves [7] propagating away from the contact point as shown in Fig. 4. The compression waves travel faster in the syringe than in the liquid, and both waves create stresses and strains in the syringe as shown in Fig. 5. The transient pressure and stress waves created by abrupt syringe deceleration are analogous to the water hammer events which can occur in plumbing systems when a valve is abruptly closed [26].

2.3 Impulsive Acceleration of the Plunger-Stopper (Event 3)

The extrusion of the liquid results from the pressurization of the liquid by the force of the spring-actuated driving rod on the plunger-stopper, as shown in panel D of Fig. 1. In some devices, the driving rod will accelerate to a substantial velocity, 6 to 8 m/s, before impacting the plunger-stopper. When there is no air gap between the plunger-stopper and the liquid, the impulsive acceleration resulting from the impact of the driving rod on the plunger-stopper results in the impulsive acceleration of the liquid immediately adjacent to the plunger-stopper. This produces a compression wave

[1] One common example of this type of pressure and stress transient is when a beer bottle is broken upon its abrupt acceleration. The abrupt acceleration can be generated by holding the open bottle with one hand, and impacting on the lip of the bottle with the other hand.

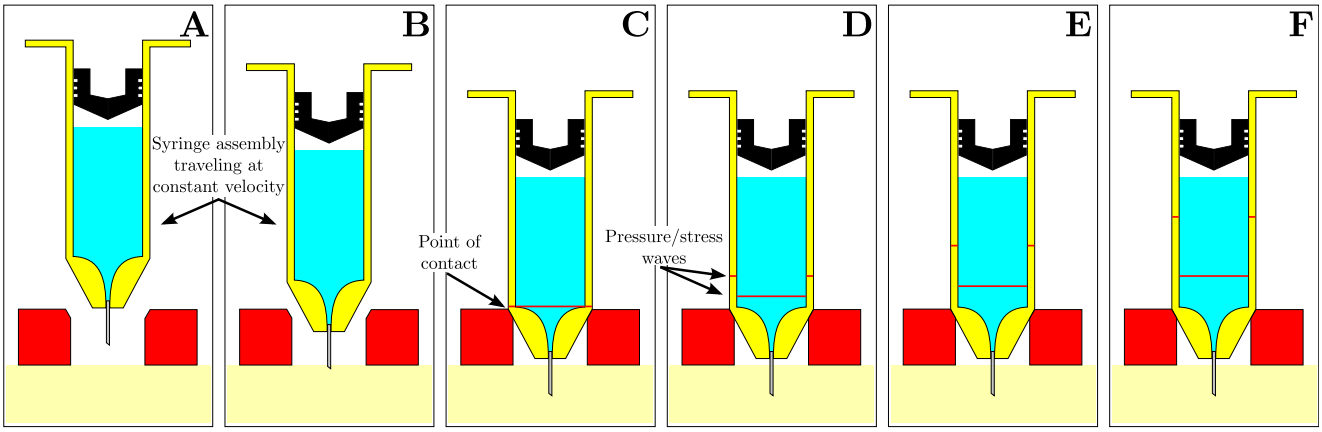

Fig. 4 Simplified schematic showing the rapid deceleration of the syringe when it reaches its travel limit. The propagation of the pressure and stress waves resulting from the rapid deceleration is shown.

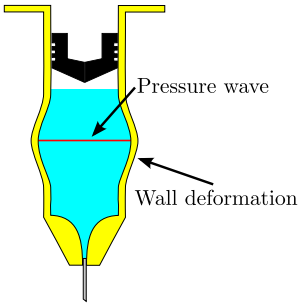

Fig. 5 Radial deformation of the syringe resulting from its interaction with a pressure wave in the liquid. The drawing is not to scale, and the deformation of the syringe is exaggerated.

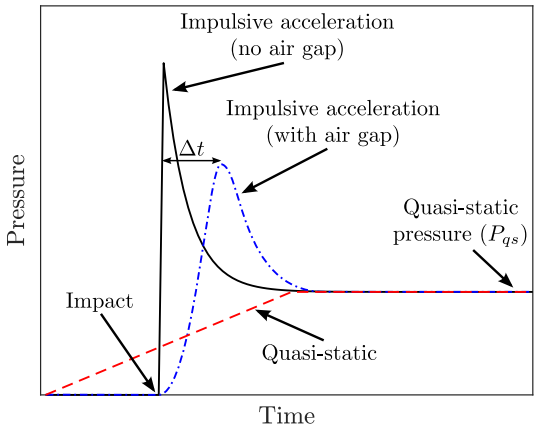

Fig. 6 Pressure history along the barrel of the syringe upon application of a force F on the plunger-stopper. The dashed curve is for a quasi-static application of the force F. The continuous and the dashed-dot curves are respectively for the impulsive application of the force F on the plunger-stopper without and with an air gap.

which propagates in the liquid away from the plunger-stopper. The liquid pressure sharply increases upon arrival of the compression wave as shown in Fig. 6. Following the sharp increase, the pressure slowly decays to a quasi-static value P_{qs} which results from the quasi-static spring force applied on the plunger-stopper.

When an air gap is present between the plunger-stopper and the liquid the syringe is pressurized through the slow, isentropic compression of the air gap. This results in a less abrupt pressure increase which now occurs over a non-zero time Δt as depicted in Fig. 6.

The pressure peak shown in Fig. 6 can have a much higher magnitude than is needed to extrude the liquid, even for drug solutions with small syringeability. The pressure peak can be eliminated by applying the force to the plunger-stopper gradually as shown in Fig. 6.

3 Experimental Methods

In this section the novel experimental methods we have developed to measure the pressure and stress transients inside a minimally modified autoinjector (patent pending) are presented. The techniques presented herein are specific to the instrumentation and investigation of a SureClick autoinjector. It is however relatively straightforward to adapt the methods for the instrumentation and investigation of other autoinjector devices. The methods are described in more detail by Veilleux and Shepherd [24].

3.1 SureClick Autoinjector

Figure 7 is a simplified schematic of the device we have studied, the SureClick autoinjector used by Amgen. Note that the precise details are not represented, but only the key features; the driving rod, the spring, the syringe,

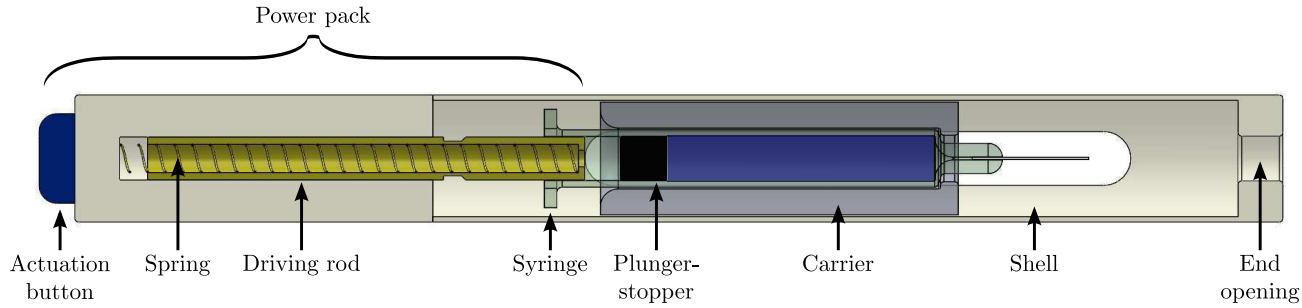

Fig. 7 Schematic of the key features of a SureClick autoinjector.

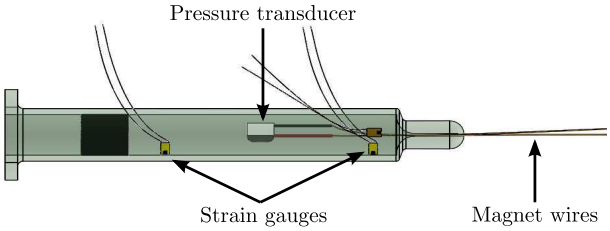

Fig. 8 Syringe instrumented with a miniature pressure transducers and miniature strain gauges.

the plunger-stopper, and the syringe carrier. Note that the spring (stiffness of 500 N/m) is initially contained within the hollow driving rod. The syringe is filled with the liquid drug solution and mounted inside a plastic carrier which is allowed to slide inside the shell. This carrier acts as a guide to ensure proper motion and alignment of the syringe. Note that no needle-insertion mechanism is shown because we found it does not play a significant role in the actuation sequence of this device.

When the user activates the device by depressing the power pack button, the internal mechanism of the power pack (not shown) releases the spring-actuated driving rod. The driving rod is then accelerated and impacts on the plunger-stopper, setting the syringe, the carrier and the liquid contained inside the syringe into motion (event 1 of section 2). This also initiates the pressurization of the syringe (event 3 of section 2). Due to the friction between the plunger-stopper and the syringe, events 1 and 3 are not entirely decoupled from one another as we assumed in the previous section. A few milliseconds after actuation the syringe carrier reaches its travel limit, and both the liquid and the syringe stop moving (event 2 of section 2). Injection of the drug into the patient then follows.

3.2 *In-situ* Measurement Technique

An essential diagnostic in studying an autoinjector is high speed imaging of the moving components. This makes it possible to verify the sequence of events and timing within the device. Quantitative image analysis enables measurements of the impact velocity between the various components, and the acceleration of the components. For high speed imaging to be possible, the shell of the autoinjector must be optically clear. In our case the optically-clear shells were fabricated through stereolithography.

Another essential diagnostic is the measurement of liquid pressure. To enable this the syringe needle is removed, and a miniature pressure transducer (e.g., PCB Piezotronics 138M186) is positioned inside the syringe. The transducer is reconnected to the amplifying electronics using magnet wires routed through the opening where the needle was attached.

The last essential diagnostic is the measurement of glass deformation (i.e., strains) in the axial and the hoop directions. The strains can be used to estimate the stresses in the glass. For this purpose miniature strain gauges (e.g., C2A-06-015LW-120 from Vishay – Micro-Measurements) are attached to the outside wall of the syringe. A schematic of the instrumented syringe is shown in Fig. 8.

The autoinjector is assembled with the instrumented syringe (see Fig. 9), and it is mounted on a special fixture to keep it steady during actuation. This is depicted in Fig. 10. Also shown are the digital high-speed camera(s) and the light source(s) adequately positioned to image the internal components of the autoinjector.

One limitation of the techniques described above is that instrumentation of the syringe is limited to its barrel. Unfortunately, the pressure transducer is too large to be installed within the conical section of the syringe. Also, the outer surface of the syringe in the vicinity of the cone and the tip of the syringe is generally irregular, and the radius of curvature is small. This makes it virtually impossible to attach strain gauges to the surface of the syringe in this region.

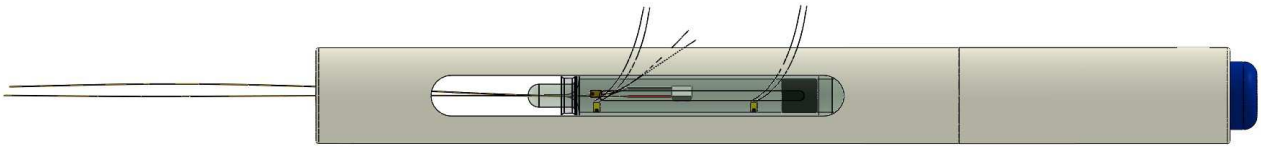

Fig. 9 Autoinjector instrumented with a miniature pressure transducer and miniature strain gauges.

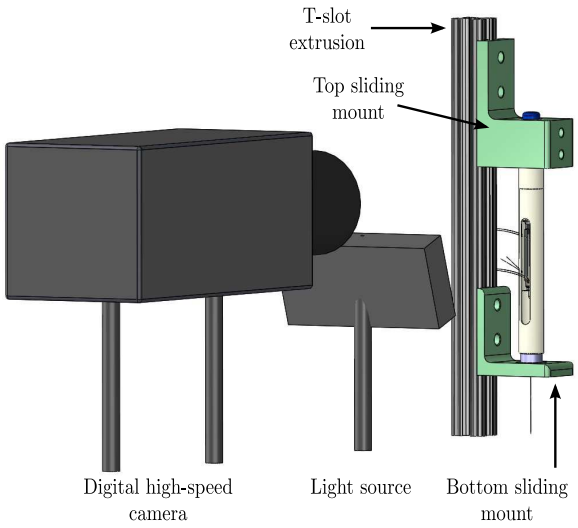

Fig. 10 Schematic showing a digital high-speed camera, a light source, and an instrumented autoinjector mounted in a special fixture before actuation.

4 Results and Discussion

In this section we provide details about two configurations which have been studied experimentally. The first case presented is for a SureClick autoinjector with a BD HyFlow 1 mL glass syringe without an air gap inside the syringe; there is a direct contact between the plunger-stopper and the liquid drug solution. The second case presented is for the same device and syringe, but with an air gap located between the plunger-stopper and the liquid drug.

In both experiments the syringe is filled with a drug solution with a viscosity of 8 to 12 cP. The exact value of the viscosity depends on the temperature of the solution. Throughout actuation the autoinjector is maintained in a vertical, tip-down configuration as depicted in Fig. 10.

The syringe is instrumented with three strain gauges positioned and oriented as shown in Fig. 8. There is one strain gauge below the plunger-stopper and one strain gauge above the cone of the syringe to measure the circumferential deformation of the glass (i.e., the hoop strains ϵ_θ). In addition, there is a strain gauge above the cone of the syringe to measure the axial deformation of the glass (i.e., the axial strains ϵ_z). The pressure transducer is located approximately half-way between the plunger-stopper and the cone of the syringe.

4.1 No Air Gap

The first configuration studied is when there is no air gap within the syringe. Multiple experiments have been performed with this configuration, but only one representative case is reported.

The position and velocity of the driving rod, the plunger-stopper and the syringe have been obtained from careful post-processing of the videos recorded using a digital high-speed camera. The position and the velocity of each component is shown in Fig. 11.

Initially, prior to actuation, all internal components of the autoinjector are at rest. Following actuation of the device the driving-rod accelerates toward the plunger-stopper. At 0 ms the driving rod impacts on the top surface of the plunger-stopper at a velocity of approximately 6.5 m/s. The initial acceleration of the plunger-stopper and the syringe following this impact event is approximately 15,000 m/s^2 or 1,500 times the gravitational acceleration. The acceleration of the syringe occurs nearly simultaneously with the acceleration of the plunger-stopper: within 0.1 ms.

The initial acceleration of the syringe is created by two mechanisms. First, there is friction between the plunger-stopper and the syringe. Second, the liquid pressure on the bottom wall of the syringe accelerates the syringe downward. When there is direct contact between the plunger-stopper and the liquid, the liquid pressure rises rapidly after the impact event, promptly initiating acceleration of the syringe. The peak internal liquid pressure during this acceleration event is approximately 2 MPa. This results in a downward force of 56 N on the syringe and the syringe carrier. The combined mass of the syringe and the syringe carrier is approximately 8 g, and Newton's Second Law of motion implies that the acceleration due to the liquid pressure applied on the syringe is about 7,000 m/s^2. This analysis indicates that friction between the syringe and the plunger-stopper as well as pressurization of the liquid are equally important in creating the initial acceleration of the syringe.

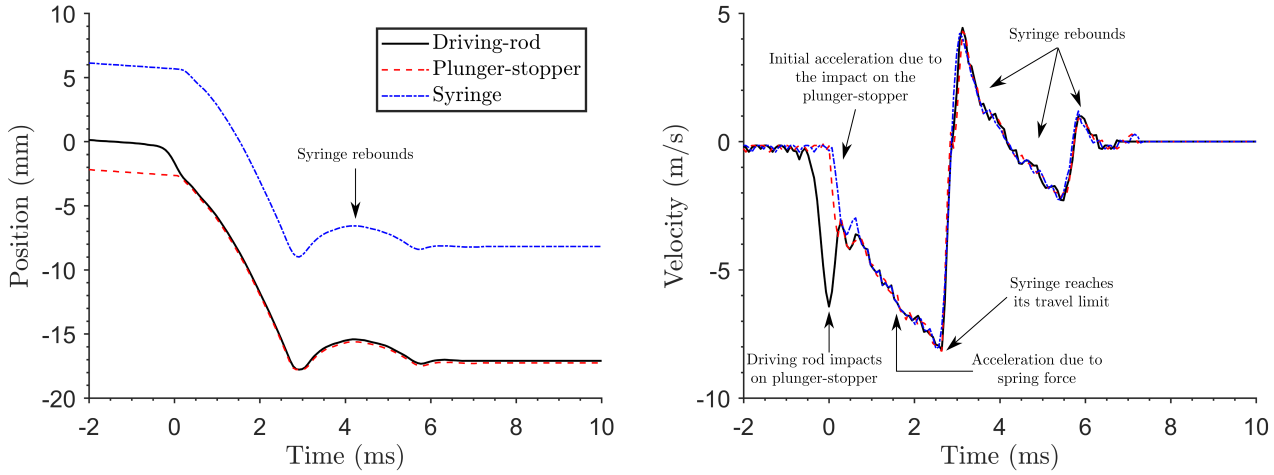

Fig. 11 Position and velocity of the moving components in a SureClick autoinjector without an air gap.

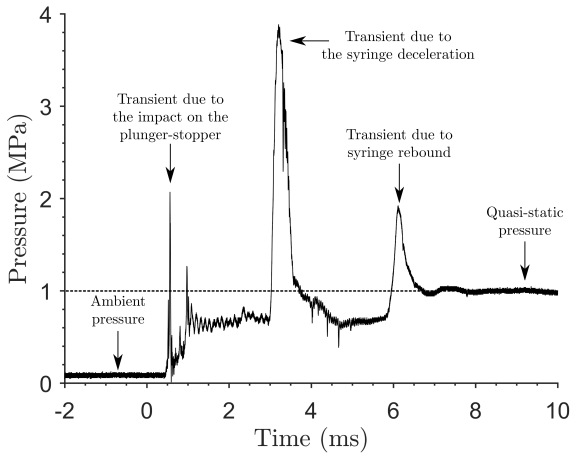

Fig. 12 Liquid pressure in a SureClick autoinjector without an air gap.

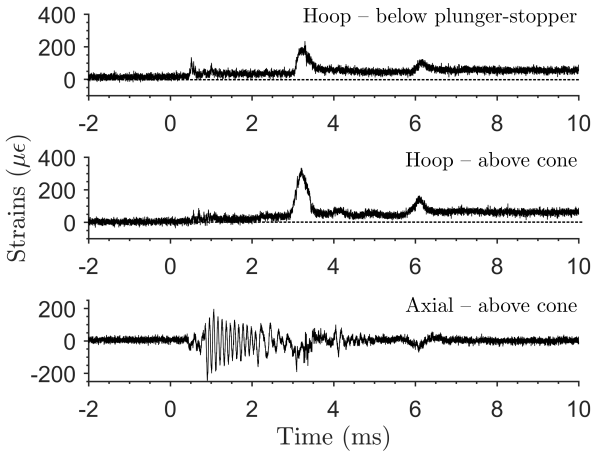

Fig. 13 Strains on the barrel of the syringe in a SureClick autoinjector without an air gap.

The initial, rapid acceleration of the syringe is followed by a much smaller acceleration of constant magnitude. This takes places between 0.75 ms and 2.5 ms, and the magnitude of the acceleration is approximately 2,000 m/s^2. During that time there is no relative motion between the driving rod, the plunger-stopper and the syringe; all components are moving together. This constant acceleration results from the steady spring force of approximately 28 N. The total mass accelerated by the spring is approximately 12.5 g. Newton's Second Law implies the expected acceleration is 2,240 m/s^2, comparable to the measured acceleration of 2,000 m/s^2.

Approximately 2.5 ms after the impact of the driving rod on the plunger-stopper, the syringe, the plunger-stopper and the driving rod are all traveling downward at a velocity of approximately 8 m/s when the syringe suddenly reaches its travel limit. All components are then rapidly decelerated; the magnitude of the deceleration is approximately 36,000 m/s^2. This means the shell of the autoinjector applies a force of 450 N on the assembly formed by the syringe and its content, the syringe carrier, the plunger-stopper, the driving rod and the spring. The assembly does not immediately come to rest after reaching its travel limit; it rebounds once between 3 ms and 6 ms. The rebound of the assembly is primarily due to the compliance of the syringe carrier and the shell of the autoinjector.

The transient events end approximately 8 ms after the impact of the driving rod on the plunger-stopper. When the syringe comes to rest, the plunger-stopper and the driving rod are pushed into the barrel of the syringe to extrude the liquid drug. The motion of the plunger-stopper and the driving rod during this quasi-static phase of the actuation is however very small (≈-

0.004 m/s), and can't be observed in Fig. 11 because of the vertical scale. The velocity of the moving components is approximately 3 orders of magnitude larger during the transient events than it is during the extrusion phase.

The liquid pressure history is shown in Fig. 12. Prior to actuation of the autoinjector the liquid drug is at atmospheric pressure. After the transient events are over (i.e., after 8 ms), the pressure in the syringe is approximately constant and equal to 1 MPa, 10 times atmospheric pressure. This is the pressure which is produced by the spring force applied on the plunger-stopper ($P_{qs} = F/A$ where A is the syringe inner cross-sectional area) to extrude the volume of liquid within an acceptable injection time. In the first 8 ms we observe 3 transient events with significant pressure excursions above the required extrusion pressure of 1 MPa.

The first excursion of the pressure occurs at around 0.5 ms when the pressure rapidly jumps to approximately 2 MPa. This pressure jump results from the impulsive acceleration of the plunger-stopper into the liquid as described in section 2 (event 3). We use acoustic theory to estimate the peak pressure rise ΔP due to the impulsive acceleration of the plunger-stopper:

$$\Delta P = \rho_l c_l w \ , \tag{2}$$

where ρ_l is the liquid density, c_l is the liquid sound speed, and w is the velocity of the plunger-stopper immediately after impact. The velocity of the plunger-stopper after impact is 3.7 m/s, and Eq. 2 predicts the peak pressure is 5.5 MPa. This is substantially more than what was measured experimentally because Eq. 2 assumes the creation of pressure waves in the liquid is decoupled from the acceleration of the syringe, but this is not the case due to friction between the plunger-stopper and the syringe. For this reason Eq. 2 is an upper bound on the expected peak pressure.

Following the impulsive acceleration of the plunger-stopper, the syringe is rapidly accelerated (event 1 of section 2) creating tension waves within the liquid. This results in the pressure dropping immediately after the driving rod impact event, another factor in the reduction of the peak pressure from the ideal value predicted by Eq. 2. In the present case of no air gap, the liquid is pressurized before the syringe is accelerated. This has the important consequence that the tension waves produced through syringe acceleration are not sufficient to reduce the pressure below the vapor pressure. The cavity formation shown in Fig. 2 is suppressed, and the pressure transient shown in Fig. 3 is eliminated.

The second excursion of the pressure occurs between 2.5 and 3.5 ms, resulting from the rapid deceleration of the syringe (event 2 of section 2). During the deceleration of the syringe the liquid pressure reaches 4 MPa, or 40 times atmospheric pressure. This is a pressure which is 4 times larger than the pressure needed to extrude the drug solution.

The third excursion of the pressure occurs between 6 and 7 ms, and results from the rebound of the syringe. The origin of this transient event is identical to that of the transient taking place between 2.5 and 3.5 ms: it is due to the deceleration of the syringe after the rebound. The maximum pressure due to this second deceleration of the syringe is approximately 2 MPa. This is two times less than the peak pressure observed during the first deceleration because the deceleration is of lesser magnitude.

The strain signals are shown in Fig. 13. A strain gauge measures the ratio of total deformation to the initial dimension of the material to which it is attached ($\epsilon = \Delta L/L$). The strains are indicated in micro-strains ($\mu\epsilon$), and 1 $\mu\epsilon$ corresponds to a deformation of 1×10^{-4} %. A positive strain indicates the material is being stretched or is under tension, and a negative strain indicates the material is being compressed.

Hoop strain signals exhibit the same features as the pressure signal because the circumferential deformation of the syringe is primarily caused by the liquid pressure. The circumferential deformation is initially zero because the liquid is initially at atmospheric pressure. After the transient events (i.e., after 8 ms) there is a residual, positive hoop strain of approximately 50 - 60 $\mu\epsilon$. The residual hoop strain is due to the pressure of 1 MPa that is required for drug solution extrusion. This can be confirmed using a static shell theory to relate hoop strains and internal pressure [13]:

$$\epsilon_\theta = \frac{PR}{h}\frac{(1-\nu^2)}{E} \ , \tag{3}$$

where R is the average radius of the syringe, h is the thickness of the syringe's walls, and E and ν are respectively the Young's modulus and the Poisson's ratio of the syringe material. Equation 3 predicts a hoop strain of 52 $\mu\epsilon$ for an internal pressure of 1 MPa; this strain is in reasonable accord with the observed values.

The initial pressure transients in the syringe result in much larger hoop strains, up to 320 $\mu\epsilon$, or over 6 times the strains observed during the extrusion phase of operation. The largest peak value of the hoop strains occurs when the syringe is rapidly decelerated, and the liquid pressure is maximum. The peak hoop strain is larger at the bottom of the syringe, in the vicinity of the cone area where the point of contact between the syringe and the shell of the autoinjector is located.

The expansion of the syringe in the circumferential direction due to the internal pressure causes the glass

to contract in the axial direction. This is known as the Poisson effect [11]. Under a uniaxial stress, when only one stress component is non-zero, there is a simple relation between the axial and the hoop strains [11]:

$$\epsilon_z = -\nu\epsilon_\theta \ . \tag{4}$$

It is possible to use the results from Fig. 13 to show that Eq. 4 is reasonably well verified before 2.5 ms and after 8 ms, which suggests the hoop stress is the dominant stress component during those time periods.

The high frequency oscillations in the axial strains observed between 0.75 ms and 2.5 ms have not been explained yet. This could result from the excitation of a natural frequency of the coupled system formed by the syringe carrier, the syringe, and the liquid it contains. This could also be the result of an interaction between the syringe and the shell into which it is sliding.

The axial strains resulting from the rapid deceleration of the syringe at around 2.5 ms are more complex. A part of the axial strains again results from the Poisson effect: the large internal pressure creates a circumferential deformation which, in turn, creates an axial deformation. There is however an additional component to the axial strains which comes from the stress wave generated within the glass itself as the syringe is decelerated. This stress wave originates from the 450 N force which is applied on the syringe assembly at the point of contact with the shell of the autoinjector.

It is possible to estimate the peak axial stress σ_z in the glass upon the rapid deceleration of the syringe as:

$$\sigma_z = -2\rho_s L a \ , \tag{5}$$

where ρ_s is the density of the glass, L is the length of the syringe barrel, and a is the magnitude of the deceleration. This estimate has been obtained using stress wave theory [14]; Eq. 5 is obtained by solving the wave equation (this is shown in Appendix A). Equation 5 predicts a peak axial stress of -8.3 MPa for an acceleration of 36,000 m/s^2, and a glass syringe barrel length of 50 mm.

The stresses in the syringe are inferred from the measured strains shown in Fig. 13. The calculation uses Hooke's law assuming plane stress [3]. For the plane stress assumption to be valid requires the radial stress to be negligible relative to the axial and hoop stresses. This will be verified *a posteriori*. The hoop (σ_θ) and axial (σ_z) stresses are:

$$\sigma_\theta = \frac{E}{1-\nu^2}\left(\epsilon_\theta + \nu\epsilon_z\right) \ , \tag{6}$$

$$\sigma_z = \frac{E}{1-\nu^2}\left(\epsilon_z + \nu\epsilon_\theta\right) \ . \tag{7}$$

The maximum hoop stress is $\sigma_\theta \approx 22$ MPa, and the maximum axial stress is $\sigma_z \approx$ -8.3 MPa. The maximum axial stress is in agreement with the value obtained using Eq. 5.

The radial stress on the outer wall of the syringe barrel, where the measurements were performed, is due to atmospheric pressure alone. The radial stress σ_r on the outer wall is $\approx$ -0.1 MPa, which is small compared to the hoop and axial stresses. This suggests the plane stress assumption is justified.

The failure of glass, a brittle material, is generally predicted using the maximum principal stress theory [3, 11]. The theory states that failure occurs when the maximum principal stress σ_1 exceeds the uniaxial tensile strength of the material. The principal stresses $\sigma_1 > \sigma_2 > \sigma_3$ are obtained through diagonalization of the stress tensor [3].

In our experiments we have not measured the principal stresses, but from both finite-element simulations and the Lamé solution for a long cylinder under pressure [3] we know that the shear stresses are negligible along the barrel of the syringe. Therefore, $\sigma_1 \approx \sigma_\theta$, and we infer the peak value of the maximum principal stress on the outer wall of the syringe is 22 MPa. The stresses on the inner surface of the barrel in the vicinity of the cone (to be discussed later), where stress concentrations will occur, or where the shear stresses are non-negligible, can be significantly larger than 22 MPa.

The magnitude of the stress is one of several factors to consider in evaluating the potential for the failure of the syringe. A complete assessment of the probability of glass failure is challenging [5, 17]. Glass is a brittle material which fails in tension, and its failure is mainly governed by the presence of microscopic flaws where stress concentration occurs [5]. There exists a large gap between the theoretical strength and the practical strength of glass. There is also great variability in the permissible working stress, the value of which is influenced by factors such as the type of glass, the condition of the glass and its surface, and the heat or chemical treatment applied during manufacturing [17]. Typical values of the working stress of glass can vary somewhere between 6 MPa and 90 MPa [17]. This suggests the transient events taking place within the syringe produce tensile stresses which are capable of causing failure of the glass syringe at a low but detectable occurrence rate.

To summarize, pressure and strain measurements have been performed along the barrel of a syringe without an air gap between the plunger-stopper and the liquid drug. We found that the transient events taking place within the first 8 ms of device actuation can

result in significant accelerations and decelerations of the components, and in substantial impact velocities. As a consequence the instantaneous pressure reaches values which are up to 4 times higher than the pressure required for drug extrusion. These transient internal pressure creates measurable strains within the syringe, and we infer that significant stresses are created within the glass. The impact of the syringe on the shell of the autoinjector also creates strains and associated stresses within the syringe. Overall, the stresses are large enough to be considered as a potential factor in the syringe failures that have occurred during patient use of autoinjectors.

4.2 With an Air Gap

The second configuration studied is when there is an air gap within the syringe. Multiple experiments have been performed with various air gap sizes, but only one representative case with an initial air gap size δ_0 of 3 mm is reported and discussed. We recall the autoinjector is in a vertical, tip-down configuration meaning the air gap is initially located between the plunger-stopper and the liquid drug solution.

The position and velocity of the driving rod, the plunger-stopper and the syringe are shown in Fig. 14. There is a gap in the syringe's motion data between 1.6 ms and 2.2 ms because the motion of the plunger-stopper and the driving rod is not accessible throughout the entire test. Data from other tests has shown that the plunger-stopper, the driving rod and the syringe all move together 1.25 to 1.5 ms after the impact of the driving rod on the plunger-stopper.

The impact of the driving rod on the plunger-stopper occurs at 0 ms. There are noticeable differences between Fig. 11 (no air gap) and Fig. 14 (with an air gap). One difference is the change in timing between plunger-stopper and syringe acceleration. Without an air gap the syringe and the plunger-stopper are accelerated together at the same rate, but this is not the case when an air gap is present.

Just after impact of the driving rod on the plunger-stopper the acceleration of the plunger-stopper is approximately 27,000 m/s^2, and the acceleration of the syringe is approximately 7,000 m/s^2. The acceleration of the plunger-stopper is almost twice as large as for the no-air-gap case due to the damping effect of the air gap; the pressure within the air gap takes a relatively long time to increase. Without an air gap the pressure below the plunger-stopper increases abruptly after impact, immediately accelerating the liquid and the syringe.

The acceleration of the syringe with an air gap is approximately 50% smaller than the acceleration of a syringe without an air gap. Because the air gap pressure and the liquid pressure slowly increase when there is an air gap, acceleration of the syringe results almost entirely from the friction between the syringe and the plunger-stopper. With an air gap the liquid pressure applied at the bottom of the syringe only contributes minimally to the acceleration of the syringe.

Deceleration of the syringe is observed between 0.4 ms and 1 ms after the impact event. The magnitude of the deceleration is approximately 8,000 m/s^2. We have studied in separate tests the motion of the syringe carrier (not shown) and found that the deceleration results from an elastic interaction between the syringe and the carrier. The deceleration of the syringe upon reaching its travel limit at approximately 2.8 ms is 26,000 m/s^2. The characteristics of this deceleration are almost identical to the no-air-gap case, but it is of lesser magnitude.

The liquid pressure is shown in Fig. 15. The events taking place after 2.5 ms (i.e., the transients due to syringe deceleration and syringe rebound) are very similar to what has been observed and discussed without an air gap. This, along with the results from other experiments, suggests the deceleration of the syringe and the other moving components is relatively insensitive to the presence of an air gap between the plunger-stopper and the liquid. In this test, the baseline of the pressure transducer signal shifted during actuation of the autoinjector. As a consequence, the extrusion pressure is incorrectly registered as 0.4 MPa, which is inconsistent with the hoop strains in the syringe (see Fig. 16). Using the hoop strains we infer the extrusion pressure to be around 1 MPa.

The transient events taking place within the first 2.5 ms following impact of the driving rod on the plunger-stopper are different from what was observed without an air gap. The pressure does not increase immediately after the impact of the driving rod on the plunger-stopper, but instead *decreases*. This pressure decrease is caused by the syringe acceleration which creates tension waves as discussed in section 2 (event 1).

With an air gap, pressurization of the liquid does not occur before the syringe is substantially accelerated. Without pre-pressurization of the liquid, the tension waves are sufficient to reduce the liquid pressure to sub-atmospheric values, which results in transient cavitation: bubbles form, grow and collapse. One such rapid bubble collapse occurs at 0.8 ms. This results in the production of a sharp and substantial pressure wave with a magnitude close to 10 MPa, or 100 times atmospheric pressure (10 times the pressure needed for the extrusion phase). The oscillatory pressure signal indi-

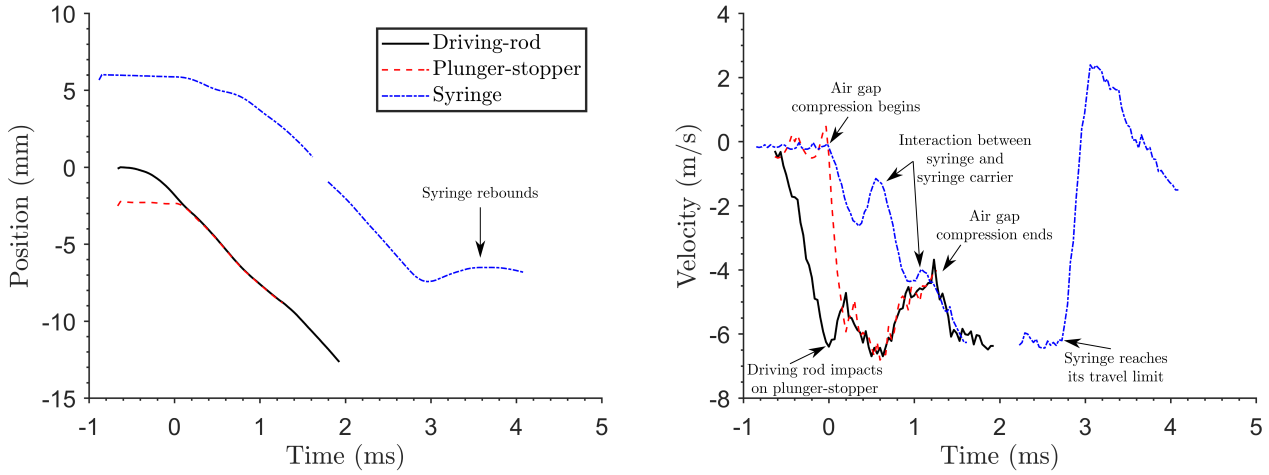

Fig. 14 Position and velocity of the moving components in a SureClick autoinjector with an air gap.

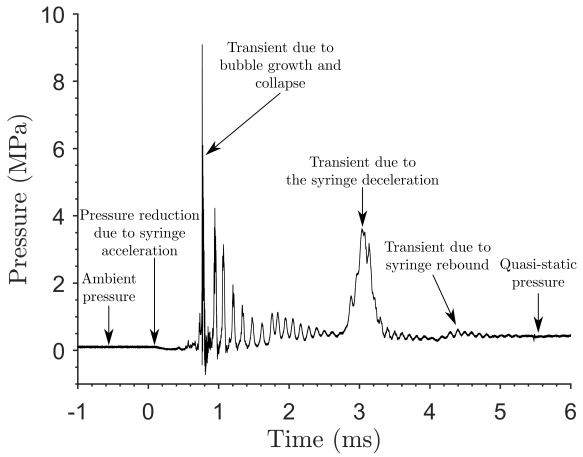

Fig. 15 Liquid pressure in a SureClick autoinjector without an air gap.

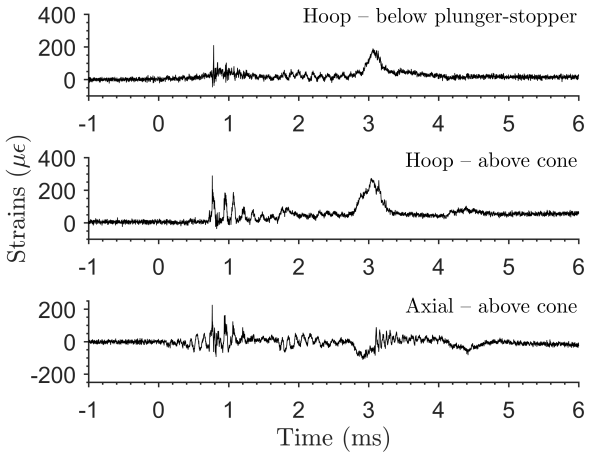

Fig. 16 Strains on the barrel of the syringe in a SureClick autoinjector without an air gap.

cates that the bubbles grow and collapse multiple times, resulting in successive sharp peaks of decaying amplitude. It has been confirmed using high speed imaging that cavitation is indeed responsible for these features of the pressure trace.

To obtain clearer images of the bubble dynamics due to cavitation, an experiment has been performed with a non-instrumented syringe. A sequence of images showing the growth and collapse of a cavitation bubble within the cone of the syringe is shown in Fig. 17. Bubble growth begins at frame 1 when acceleration of the syringe begins. The cavity grows for approximately 360 μs or until frame 13. The collapse of the cavity is rapid (within 60 μs), and occurs over the span of 2 frames (frames 14 and 15).

When an air gap is present the large acceleration of the syringe consistently causes bubbles or cavities to form and collapse in the cone of the syringe. Cavitation bubbles can also form away from the cone as illustrated in frame 4 of Fig. 17. As expected, the exact location of bubble growth and collapse varies between experiments. Cavitation bubbles collapsing close to a wall can produce significant wall stresses [4].

The hoop and axial strains are shown in Fig. 16. The distinctive signature of the collapsing bubble is visible on the hoop strains measured above the cone of the syringe. One would however expect the peak hoop strains to be larger than 300 $\mu\epsilon$ in order to be consistent with the peak pressure of 10 MPa. We recall the peak hoop strains were approximately 320 $\mu\epsilon$ for a peak pressure of 4 MPa when there was no air gap.

This inconsistency can be explained by the location of the collapse relative to the strain gauge. The collapsing bubble which produced the large pressure signal of

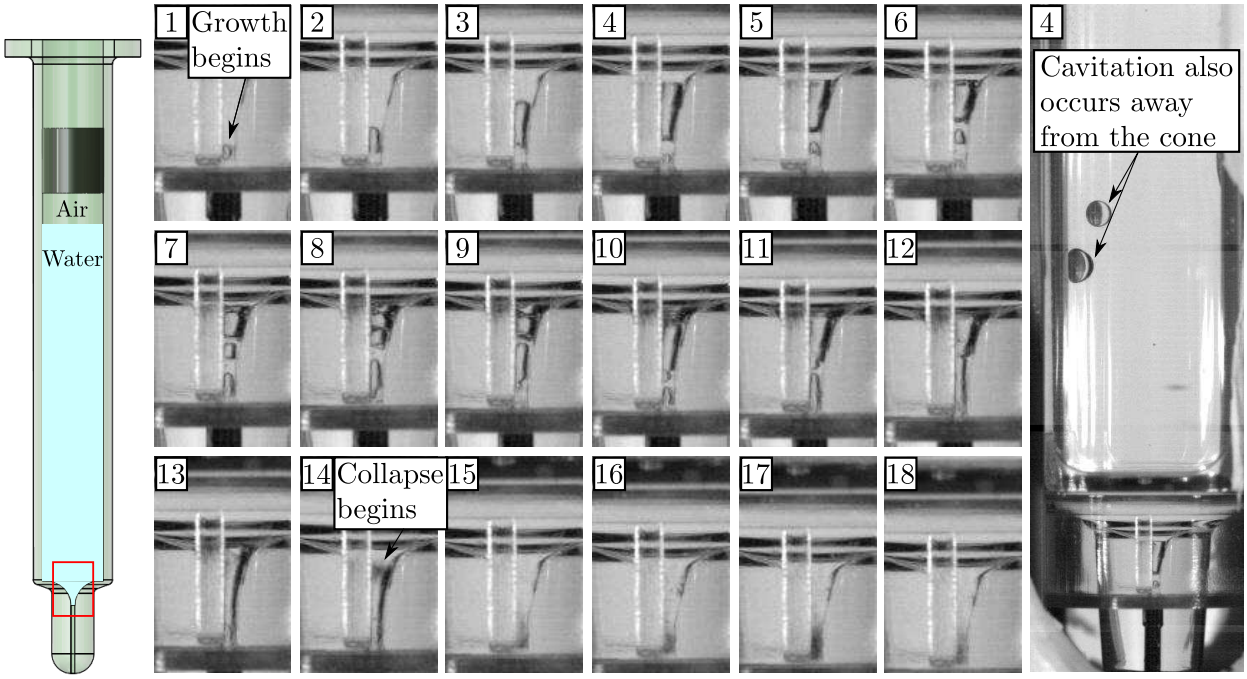

Fig. 17 Growth and collapse of a cavity in the cone area and evidence of cavitation occuring outside the cone during device actuation (frames separated by 30 μs).

10 MPa was very close to the pressure sensor, but relatively far from the strain gauges. Following the collapse and rebound of a cavitation bubble, a spherical shock wave is produced and propagates away from the bubble. The magnitude of the spherical wave decays rapidly as it travels away from the bubble [4].

The strain gauge located below the plunger-stopper does not exhibit the distinctive signature of cavitation in the form of multiple pressure peaks. This is because that strain gauge was essentially responding to the air gap pressure which is isolated from the weakened cavitation pressure pulses arriving at this location.

In summary, the presence of an air gap between the plunger-stopper and the liquid modified the timing between pressurization and acceleration of the syringe. With an air gap the acceleration takes places before the liquid pressure increases, and cavitation occurs. The collapse of the cavitation bubbles can create significant, but highly localized pressures within the liquid. The collapse of a bubble close to a wall can result in substantial wall stresses capable of causing failure of the syringe. The pressure and stresses transients generated upon deceleration of the moving components occurring when the syringe reaches its travel limit are not significantly affected by the presence of an air gap.

4.3 Pressure in the Cone

Until now we have studied and discussed the transients using measurements performed along the barrel of the syringe. The pressure inside the cone of the syringe can however be significantly different from the pressure in the barrel of the syringe due to shock focusing. The small size of the cone makes it difficult with our existing instrumentation to perform spatially resolved measurements of the pressure inside the cone. Instead, numerical simulations have been performed using the LS-DYNA software [12] to investigate and quantify shock focusing.

A cross-sectional view of the geometry used in the numerical simulations is shown in Fig. 18. The left-hand-side of Fig. 18 shows the initial configuration: a shock wave is traveling downward in a syringe-like geometry filled with water. The diameter of the barrel is D, the diameter of the tip wall is d, and the cone has a constant half-angle α. Ahead of the shock wave the pressure is P_0, and behind the shock wave the pressure is P_s. The shock wave is weak (i.e., $P_s \ll \rho_l c_l^2$) and can be considered an acoustic disturbance traveling at sound speed c_l.

All simulations were performed in 2D axisymmetric mode using an inviscid solver. The contraction ratio

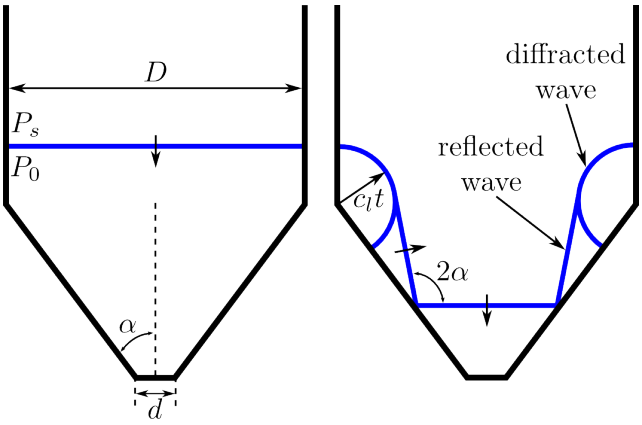

Fig. 18 Cross-sectional view of the geometry used in the numerical simulations. The left-hand-side is the initial configuration, and the right-hand-side is the situation after the shock wave has entered the cone.

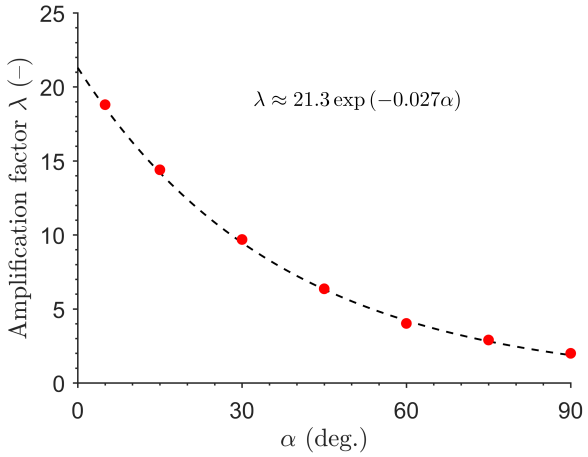

Fig. 19 Evolution of the amplification factor of the cone with half-angle α.

D/d is equal to 9. The pressure rise across the shock was arbitrarily set to $P_s - P_0 = 1$ MPa. The half angle α was varied between 5 and 90 deg. The computational grid is constructed using 750,000 to 2,250,000 shell elements depending on the half-angle α.

The right-hand-side of Fig. 18 illustrates the physical situation after the shock wave has entered the cone. When the incident shock wave enters the cone, a reflected and a diffracted wave form. Because this is an acoustic problem the reflection of the incident wave on the wall is regular [6], and the angle between the wall and the incident wave is the same as the angle between the wall and the reflected wave. The diffracted wave forms as a result of the wave turning the corner between the straight section of the syringe and the cone.

The reflected and the diffracted waves converge toward the axis of symmetry of the cone. This means some of the energy transported by the waves is focused on the axis of symmetry. Although it is typical to think of pressure as a force per unit area (N/m^2), it is also possible to think of pressure as an energy density (J/m^3). It then becomes easier to understand the amplification mechanism: the focusing of the energy transported by the shock waves on the axis of symmetry increases the energy density. This, in turn, translates into a substantial increase in liquid pressure.

We now define the pressure P_{tip} to be the spatial average of the pressure over the tip region of diameter d. The maximum value of P_{tip} is used to define an amplification factor λ which quantifies the shock focusing effect taking place within the cone:

$$\lambda = \frac{(P_{tip})_{max}}{P_s} \ . \tag{8}$$

Values of λ for various half-angles α are shown in Fig. 19. The case $\alpha = 90$ deg. corresponds to the situation where no cone is present: the syringe is terminated by a flat wall. For this case, acoustic theory [18] predicts an amplification factor should be $\lambda = 2$, and this is indeed what has been obtained through numerical simulations.

The numerical simulations suggest the amplification factor increases exponentially as the half-angle of the cone is reduced. This means a deeper cone which converges at a shallower angle tends to focus more energy at its tip. The exponential relation between λ and α is expected to depend on the contraction ratio D/d.

The numerical results demonstrate the cone of a syringe can substantially amplify sharp pressure waves. Earlier we reported the measurement of peak pressures around 10 MPa upon the intense collapse of a cavitation bubble. When such an intense collapse occurs in the vicinity of the cone, the resulting sharp pressure waves will travel into the cone, they will be amplified, and the wall stresses in the cone could be much larger than what has been measured along the barrel of the syringe.

The simplified geometry used in the simulations reported above is not exactly that of an actual pre-filled syringe. In most pre-filled syringes the half-angle is not a constant, but varies with axial location. A simulation was performed with the nominal geometry of a BD HyFlow 1 mL pre-filled syringe. Initially, the magnitude of the incident shock wave is 1 MPa. A sequence of images showing the evolution of the pressure and the displacement of the wave fronts is shown in Fig. 20. The left-hand-side of each panel illustrates the location of the incident, reflected and diffracted wave fronts (the color scale is not meaningful). The right-hand-side of each panel depicts the pressure field using the color scale shown at the top of Fig. 20.

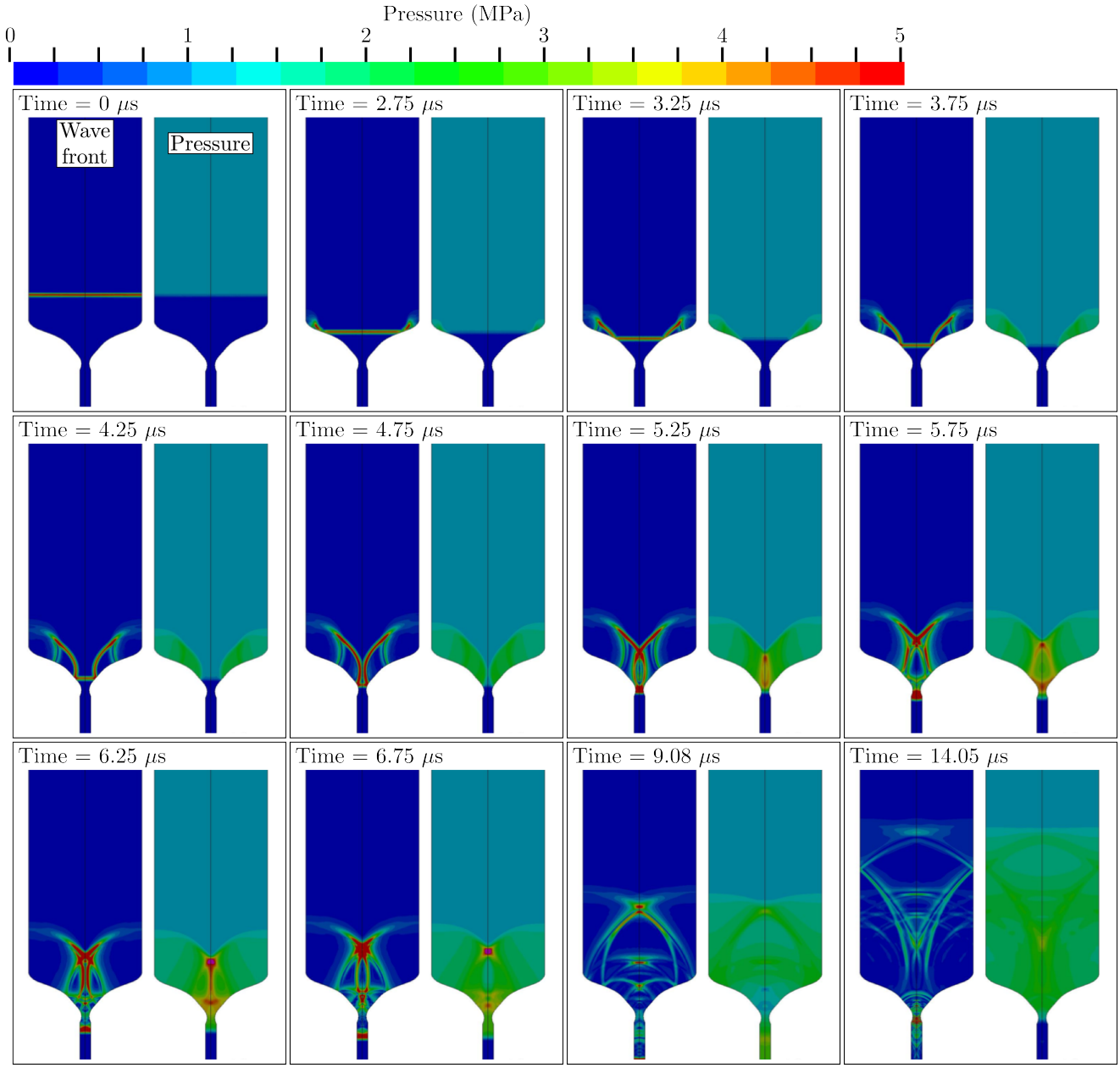

Fig. 20 Amplification of a sharp pressure wave in the conical section of a BD HyFlow 1 mL pre-filled syringe.

Between 2.75 and 4.75 μs the diffracted wave and the reflected wave form and converge toward the axis of symmetry. While this occurs, the pressure becomes non-uniform in the radial direction; the pressure is larger in the vicinity of the axis of symmetry. Between 5.75 and 6.75 μs a region of substantial pressure develops in the cone of the syringe where the cross-sectional area is minimum. The pressure there is approximately 5 MPa, or 5 times larger than the initial magnitude of the pressure wave prior to entering the cone.

To summarize, numerical simulations have shown the potential for significant amplification of sharp pressure waves as they travel into the conical geometry terminating the syringe. The amplification results from a geometrical effect which tends to focus the energy on the axis of symmetry. The magnitude of the amplification depends on the detail of the geometry of the cone, but shallower half-angles tend to create a larger amplification effect. An amplification factor of approximately 5 has been predicted for a typical pre-filled syringe geometry.

5 Conclusion

The actuation of a typical autoinjector can be separated in two phases: 1) the transient phase; 2) the extrusion phase. The transient phase is generally very short (i.e., a few miliseconds), and the extrusion phase is typically long (i.e., a few seconds). The extrusion phase is simple to understand since it is quasi-static and a dynamic analysis is not required. During the extrusion phase, the liquid pressure $P = F/A$ produced by the spring-force is essentially constant in time. On the contrary, the transient phase is composed of highly dynamic events creating transient pressures within the drug solution, and rapidly changing stresses in the syringe.

We have found there are three types of events which can occur during the transient phase to create substantial pressures and stresses: 1) the large acceleration of the syringe; 2) the large deceleration of the syringe; 3) the impulsive application of a force on the plunger-stopper. Although the origin and the nature of each transient event is different, they can all produce pressures and stresses in the syringe which are far in excess of what is needed for the normal operation of the autoinjector. In any case, the instantaneous pressure and stresses are much larger during the transient phase than they are during the extrusion phase.

We developed novel experimental techniques to measure the pressure and stress transients within a minimally modified autoinjector. The syringe was instrumented with a miniature pressure transducer and multiple miniature strain gauges. High speed digital cameras are also used to visualize the motion of the various components during actuation.

We applied these techniques to study the transient phase in a SureClick autoinjector. We found that the presence of an air gap is a key parameter and substantially affects the transient events. This is because the presence and size of an air gap controls the relative timing between pressurization and acceleration of the syringe.

Without an air gap, pressurization and acceleration of the syringe occur almost simultaneously. No cavitation takes place in the syringe, and we observed peak pressures which are 4 times larger than the pressure needed for the timely extrusion of the drug. When there is an air gap, pressurization of the syringe happens after its acceleration. Cavitation is observed, and the maximum liquid pressure results from the rapid collapse of cavitation bubbles. Liquid pressures 10 times larger than what is needed to achieve the normal functions of the device have been observed.

Numerical simulations have been performed to understand the pressure field in the cone of the syringe. We were able to demonstrate that shock focusing of sharp pressure waves can occur in the conical section terminating the syringe. This can result in liquid pressures which are much larger in the cone than in the barrel of the syringe. The tensile hoop stresses which are produced by the large liquid pressure, especially in the cone of the syringe, can cause failure of the glass syringe at a low but detectable rate. Additional numerical simulations are in progress to predict the complete stress field in the vicinity of the cone.

The magnitude of the pressure and stresses during the transient phase can be substantially diminished by reducing the acceleration/deceleration of the components. Reducing the impact velocities between the moving components is also effective in diminishing the peak pressure and stresses. Although we did not report on mitigation techniques in this paper, we have developed a damping system which proved successful at reducing the magnitude of the pressure and stress transient. This is discussed by Veilleux and Shepherd [24].

Acknowledgements

This work is sponsored by Amgen through the Caltech-Amgen Research Collaboration Agreement for Chem-Bio-Engineering Awards. We would like to thank Julian Jazayeri for his help in performing some of the experiments. We would also like to thank Julian Jazayeri and Dr. Bruce Eu for their support and fruitful discussions.

Compliance with Ethical Standards

J.C. Veilleux is listed as a co-author on a U.S. patent application related to the content of this work. J.E. Shepherd is listed as a co-author on a U.S. patent application related to the content of this work, and has consulted for Amgen in 2014 and 2015.

References

1. Adler, M.: Challenges in the Development of Prefilled Syringes for Biologics from a Formulation Scientist's Point of View. American Pharmaceutical Review. (2012). `http://www.americanpharmaceuticalreview.com/`. Accessed April 6, 2018
2. Akers, M.J.: Sterile Drug Products: Formulation, Packaging, Manufacturing and Quality, 1st edn. Drugs and the Pharmaceutical Sciences Series. CRC Press (2010)
3. Bower, A.: Applied Mechanics of Solids, 1st edn. CRC Press (2009)
4. Brennen, C.: Cavitation and Bubble Dynamics. Oxford Engineering Science Series. Oxford University Press (1995)

5. Callister, W.D., Rethwisch, D.G.: Materials Science and Engineering : an Introduction. John Wiley and Sons, Hoboken, NJ (2014)
6. Courant, R., Friedrichs, K.: Supersonic Flow and Shock Waves, 1st edn. Applied Mathematical Sciencess. Springer-Verlag New York (1976)
7. Davis, J.: Wave Propagation in Solids and Fluids. Springer-Verlag (1988)
8. Franc, J., Michel, J.: Fundamentals of Cavitation. Fluid Mechanics and Its Applications Series. Springer Netherlands (2006)
9. French, D., Collins, J.: Advances in Parenteral Injection Devices and Aids. In: S. Nema, J. Ludwig (eds.) Pharmaceutical Dosage Forms: Parenteral Medications, 3rd edn., pp. 71–85. Informa Healthcare (2010)
10. Fry, A.: Injecting Highly Viscous Drugs. Pharmaceutical Technology **38**(11) (2014)
11. Hibbeler, R.: Mechanics of Materials, 8th edn. Prentice Hall, Singapore (2011)
12. J. O. Hallquist: LS-DYNA : THEORY MANUAL. Livermore Software Technology Corporation, Livermore, California (USA), latest edn. (2006). `http://www.lstc.com/manuals`
13. Jones, N.: Structural Impact. Cambridge University Press (1997)
14. Kolsky, H.: Stress Waves in Solids. Oxford University Press, London (1953)
15. Kundu, P., Cohen, I., Dowling, D.: Fluid Mechanics, 5th edn. Academic Press, Oxford, England (2012)
16. Lange, J., Thompson, I.: Self-Injection Devices. In: Encyclopedia of Pharmaceutical Science and Technology, 4th edn., pp. 3132–3143. Taylor & Francis (2013)
17. McLellan G.W., S.E.: Glass Engineering Handbook, 3rd edn. McGraw-Hill (1984)
18. Pierce, A.: Acoustics : an Introduction to its Physical Principles and Applications, 2nd edn. Acoustical Society of America (1989)
19. Schiff, M., Jaffe, J., Freundlich, B., Madsen, P.: New autoinjector technology for the delivery of subcutaneous methotrexate in the treatment of rheumatoid arthritis. Expert Review of Medical Devices **11**(5), 447–455 (2014). DOI 10.1586/17434440.2014.929492
20. Shire, S.J., Shahrokh, Z., Liu, J.: Challenges in the Development of High Protein Concentration Formulations. Journal of Pharmaceutical Sciences **93**, 1390–1402 (2004). DOI 10.1002/jps.20079
21. Stout, D., Vilivalam, V.: Plastic Prefilled Syringes: A Better Fit for Autoinjector Systems. Pharmaceutical Technology (Volume 2009 Supplement, Issue 6) (2009)
22. Thompson, I.: Self-Injection Technology and Trends. Journal of Innovations in Pharmaceutical Technology **20**, 60–63 (2006)
23. Thompson, I., Lange, J.: Pen and Autoinjector Drug Delivery Devices. In: P. Kohle, M. Shah, N. Rathore (eds.) Sterile Product Development: Formulation, Process, Quality and Regulatory Considerations, AAPS Advances in the Pharmaceutical Sciences Series, pp. 331–356. American Association of Pharmaceutical Scientists (2013). DOI 10.1007/978-1-4614-7978-9_13
24. Veilleux, J.C., Shepherd, J.: Dampers and methods for performing measurements in an autoinjector. US Patent Application 20180015224. Filed July 2017. Published January 2018.
25. Wilkins, J., Simpson, I.: Mathematical Modeling for Faster Autoinjector Design (2012). `http://www.drug-dev.com/`. Accessed April 6, 2018
26. Wylie, E., Streeter, V., Suo, L.: Fluid Transients in Systems. Prentice Hall (1993)

Appendix A.

The axial stresses in the syringe barrel when it is rapidly decelerated can be estimated using stress wave theory and acoustics [14, 18]. The estimate is obtained by assuming the stresses in the syringe during the deceleration are uniaxial, which makes it possible to approximate the syringe barrel as a one-dimensional bar. This assumption is reasonable as long as the magnitude of the axial stresses remains large compared to the magnitude of the hoop and the radial stresses.

The physical problem which needs to be solved in order to obtain the stress estimate is as follows. At time $t < 0$, the syringe barrel of length L is moving at a constant velocity U_0 in the negative z direction. At times $t > 0$ a force F is applied on the syringe end located at $z = 0$. The force F is oriented in the positive z direction and decelerates the syringe at a rate a. The end of the syringe located at $z = L$ corresponds to a stress free end.

The initial velocity U_0 of the syringe is not important in this problem, and it can be eliminated because it is the rate of change of the velocity which creates stresses. The equivalent mathematical problem is formulated using an acoustic potential $\phi(z,t)$ and necessitates solving the wave equation:

$$\phi_{tt}(z,t) = c^2\phi_{zz}(z,t) \ , \ (0 < z < L, 0 < t < \infty) \ , \quad (9)$$

$$\phi(z,0) = 0 \ \text{ and } \ \phi_t(z,0) = 0 \ , \ (0 < z < L) \ , \quad (10)$$

$$\phi_z(0,t) = at \ \text{ and } \ \phi_t(L,t) = 0 \ , \ (0 < t < \infty) \ , \quad (11)$$

where:

$$\sigma_z(z,t) = \rho_s\phi_t(z,t) \ , \quad (12)$$

and

$$u(z,t) = \phi_z(z,t) \ . \quad (13)$$

Note that c corresponds to the sound speed in the solid syringe wall. The following linear transformation is performed:

$$\phi(z,t) = \psi(z,t) - (L-z)at \ , \quad (14)$$

and the reformulated mathematical problem is:

$$\psi_{tt}(z,t) = c_0^2\psi_{zz}(z,t) \ , \ (0 < z < L, 0 < t < \infty), \quad (15)$$

$$\psi(z,0) = 0 \text{ and } \psi_t(z,0) = (L-z)a \ , \ (0 < z < L), \quad (16)$$

$$\psi_z(0,t) = 0 \ \text{ and } \ \psi_t(L,t) = 0 \ , \ (0 < t < \infty). \quad (17)$$

The solution is obtained using separation of variables. Once the solution ψ is found, the linear transformation

given by Eq. 14 is used to recover ϕ:

$$\phi(z,t) = \sum_{n=1,3,\ldots}^{\infty} \frac{16L^2 a}{c_0 n^3 \pi^3} \sin\left(\frac{n\pi c_0}{2L} t\right) \cos\left(\frac{n\pi}{2L} z\right) - (L-z)at \ . \quad (18)$$

The stresses are calculated using Eq. 12:

$$\sigma(z,t) = \rho_s \sum_{n=1,3,\ldots}^{\infty} \frac{8La}{n^2\pi^2} \cos\left(\frac{n\pi c_0}{2L} t\right) \cos\left(\frac{n\pi}{2L} z\right) - (L-z)a \ . \quad (19)$$

Because of the $\cos\left(\frac{n\pi}{2L} z\right)$ term, the maximum stresses are attained at $z = 0$, where:

$$\sigma_z(0,t) = \rho_s \sum_{n=1,3,\ldots}^{\infty} \frac{8La}{n^2\pi^2} \cos\left(\frac{n\pi c_0}{2L} t\right) - \rho_s aL \ , \quad (20)$$

and one can show this is exactly equal to the periodic extension of:

$$\sigma_z(0,t) = \begin{cases} -\rho_s act, & \text{if } 0 \le t \ge \dfrac{2L}{c} \ , \\ \rho_s a(ct - 4L), & \text{if } \dfrac{2L}{c} \le t \ge \dfrac{4L}{c} \ . \end{cases} \quad (21)$$

Thus, the peak axial stresses occurs at $t = 2L/c$ and are equal to:

$$\sigma_z(0, 2L/c) = -2\rho_s aL \ . \quad (22)$$